ACS APPLIED MATERIALS & INTERFACES

Research Article

Cite This: ACS Appl. Mater. Interfaces 2019, 11, 1503−1511

www.acsami.org

Highly Ordered 3D Microstructure-Based Electronic Skin Capable of Differentiating Pressure, Temperature, and Proximity

Jin-Oh Kim,[†,∥] Se Young Kwon,[†,∥] Youngsoo Kim,[‡] Han Byul Choi,[†] Jun Chang Yang,[†] Jinwon Oh,[†] Hyeon Seok Lee,[†] Joo Yong Sim,[§] Seunghwa Ryu,[‡] and Steve Park*,[†]

[†]Department of Materials Science and Engineering and [‡]Department of Mechanical Engineering, Korea Advanced Institute of Science and Technology (KAIST), Daejeon 34141, Republic of Korea

[§]Bio-Medical IT Convergence Research Department, Electronics and Telecommunications Research Institute (ETRI), Daejeon 34129, Republic of Korea

Supporting Information

ABSTRACT: Electronic skin are devices that mimic the functionalities of human skin, which require high sensitivity, large dynamic range, high spatial uniformity, low-cost and large-area processability, and the capacity to differentiate various external inputs. We herein introduce a versatile droplet-based microfluidic-assisted emulsion self-assembly process to generate three-dimensional microstructure-based high-performance capacitive and piezoresistive pressure sensors for electronic skin applications. Our technique can generate uniformly sized micropores that are self-assembled in an orderly close-packed manner over a large area, which results in high spatial uniformity. The size of the micropores can easily be tuned from 100 to 500 μm, through which sensitivity and dynamic range were controlled as high as 0.86 kPa^{-1} and up to 100 kPa. Our device can be printed on curvilinear surfaces and be molded into various shapes. We furthermore demonstrate that by simultaneously utilizing capacitive and piezoresistive pressure sensors, we can distinguish between pressure and temperature, or between pressure and proximity. These demonstrations make our process and sensors highly useful for a wide variety of electronic skin applications.

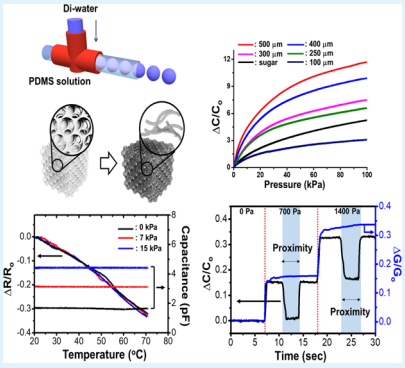

KEYWORDS: *tactile sensing, multimodal sensation, decoupled stimuli, microporous structure*

INTRODUCTION

Electronic skin (e-skin) are devices that mimic the functionalities of human skin.[1−8] They have a wide variety of applications in wearable/patchable electronics for health monitoring,[9,10] pressure-sensitive touch screens,[11] prosthetics,[7] and robotics with humanlike functionalities.[4,12−15] To properly emulate the properties of human skin, the e-skin should have high sensitivity to pressure, high dynamic range (up to 10^5 Pa), and high spatial resolution and uniformity. In addition, facile, low-cost, and large-area processability is of significant importance for commercial applicability. Furthermore, as with human skin, electronic skin should be able to distinguish various external inputs, such as pressure, temperature, and proximity (i.e., human skin achieves this using hair follicles).[16−18]

To enhance the pressure sensitivity of electronic skin, the active layer (i.e., the layer that deforms under pressure, which correspondingly dictates the change in the output signal) is often microstructured. The most commonly used method to microstructure the active layer is mold casting, through which capacitive[19,20] and piezoresistive[21,22] pressure sensors have shown improved performance. One inherent disadvantage of mold casting, however, is that a thickness of only a few hundred microns can be microstructured, limited by the etching depth and aspect ratio of the microstructural features on the mold.[19,20,22] This often results in pressure sensors with low dynamic range, where the response often saturates under pressures exceeding several tens of kilopascal.[20,22] This can be a limiting factor for e-skin applications, which requires a large dynamic range of several to hundred kilopascal.[3] Three-dimensional (3D) microstructuring of the active layer can address this issue, and several researchers have fabricated such structures by either filling in a 3D template such as sugar,[23−25] polystyrene beads,[26] and nickel foam[27,28] with the active material and subsequently etching away the template or randomly mixing aqueous and oil phases to form an emulsion and removing the solvents.[29−32]

However, these processes are either relatively costly, limiting their applicability to low-cost, large-area devices, or have randomly sized and shaped microstructures, limiting their spatial uniformity, especially for applications that require high taxel resolution.[29,30] Furthermore, it is difficult to precisely control the size of the microstructures, restricting the tunability of device performance. It is, therefore, highly important to

Received: November 2, 2018
Accepted: December 19, 2018
Published: December 19, 2018

DOI: 10.1021/acsami.8b19214
ACS Appl. Mater. Interfaces 2019, 11, 1503−1511

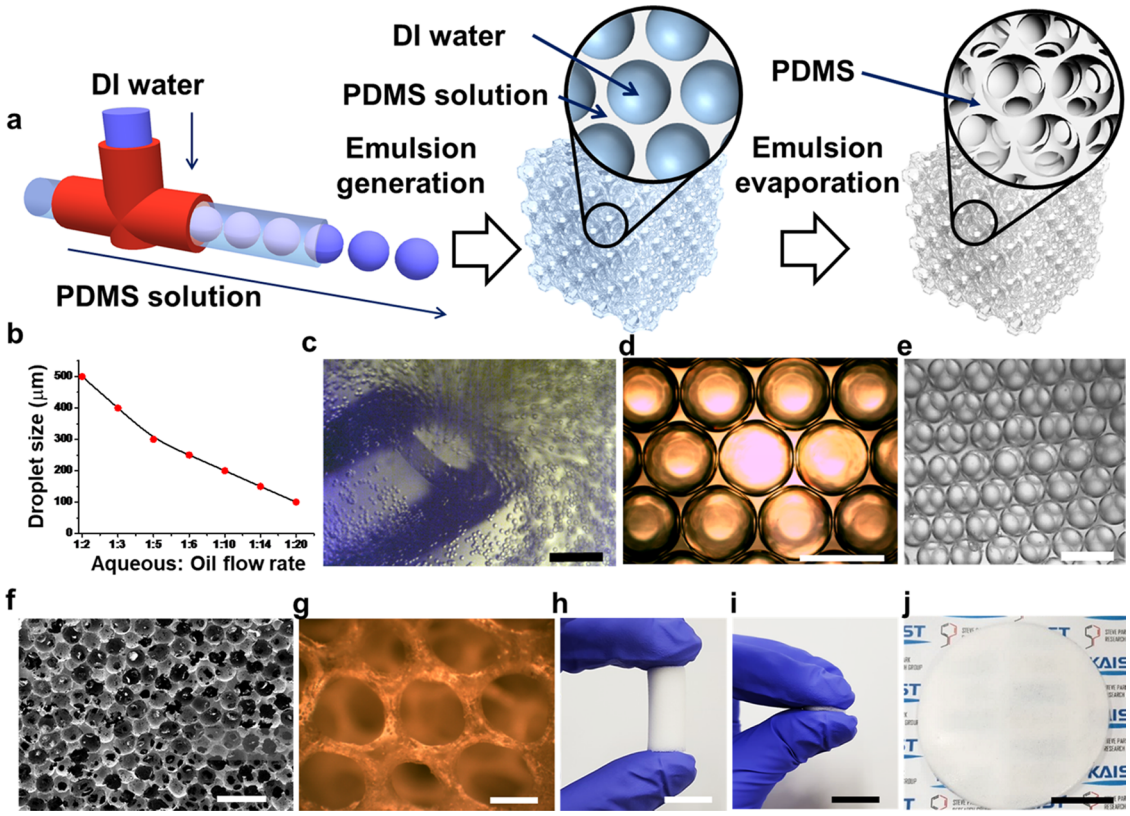

Figure 1. Fabrication process of 3D microstructure. (a) Schematic of 3D microstructured PDMS fabrication by DMESA. (b) Droplet size versus relative aqueous-to-oil solution flow rate. (c) Optical image of microdroplet generation. Optical microscopy images of (d) 500 μm and (e) 100 μm droplets assembled in closely packed hexagonal array. The scale bars are 1 mm, 500 μm, and 200 μm, respectively. (f) SEM and (g) optical image of the microstructured PDMS after curing and solvent evaporation. The scale bars are 500 and 200 μm, respectively. Volume shrinkage test of a cylindrical sample with a height of 3 cm: (h) before pressure and (i) after pressure; the scale bar is 1.5 cm. (j) Wafer-scale fabrication of microstructured PDMS by DMESA process; the scale bar is 3 cm.

develop a simple and low-cost template-free process that can generate uniformly sized 3D microstructures of variable feature sizes, along with large-area uniformity.

Herein, we introduce a novel droplet-based microfluidic-assisted emulsion self-assembly (DMESA) technique to fabricate 3D microstructured elastomer (poly(dimethylsiloxane) or PDMS) layer that can be utilized to fabricate high-performance capacitive and piezoresistive pressure sensors for electronic skin applications. DMESA process can generate uniformly sized spherical micropores, evenly assembled over a large area without the use of template, which results in high spatial uniformity. The size of the micropores can easily be tuned from 100 to 500 μm, through which the sensitivity of the pressure sensor can be controlled. To fabricate capacitive pressure sensors, the 3D microstructured elastomer itself was used as the active layer, through which sensitivity as high as 0.86 kPa^{-1} and dynamic range up to 100 kPa were achieved. To fabricate piezoresistive pressure sensors, we have functionalized the microstructured elastomer with multiwalled carbon nanotubes (MWCNTs), which also exhibited high sensitivity and large dynamic range up to 100 kPa. Finally, by utilizing both sensors, we have differentiated signals coming from pressure and temperature and from pressure and proximity. Such demonstrations of ease of processability, performance tunability, high spatial uniformity, and differentiation of various inputs render our technique highly unique and promising for many future electronic skin applications.

RESULTS AND DISCUSSION

Fabrication of 3D Microstructure Using DMESA. The fabrication process of 3D microstructured elastomer using DMESA is shown in Figure 1a. Oil solution consisting of hexadecane/PDMS/curing agent/span 80 (surfactant) and aqueous solution consisting of deionized water were prepared, as detailed in the Materials and Methods section. As seen in the left-hand side schematic of Figure 1a, the two solutions flowing through perpendicularly arranged capillary tubes met at a T-junction, where droplets of deionized water were injected into the oil (PDMS) solution. The surfactant added to the oil solution is adsorbed at the water−oil interface acting as steric barriers, thereby stabilizing the water droplets (i.e., without the surfactant, water droplets merge with each other).[33] By controlling the relative flow rates of the two solutions, the water droplet size was precisely controlled (Figure 1b) from 100 to 500 μm. Figure 1c shows an image of ejecting water droplets out of the oil solution. The water droplets are collected into a container, and since the water droplets are more dense than the oil solution, they sediment down and naturally self-assemble themselves into close-packed two-dimensional hexagonal lattice, as seen in Figure 1d. As the water droplets continue to get collected, the close-packed two-dimensional lattices stack up vertically, forming 3D close-packed structure of water droplets, as seen in Figure 1a (middle) and Figure 1e. During the PDMS curing process (heated to 80 °C for 3 h), the water evaporates, leaving behind the 3D microstructured PDMS with uniform micropore size

DOI: 10.1021/acsami.8b19214
ACS Appl. Mater. Interfaces 2019, 11, 1503−1511

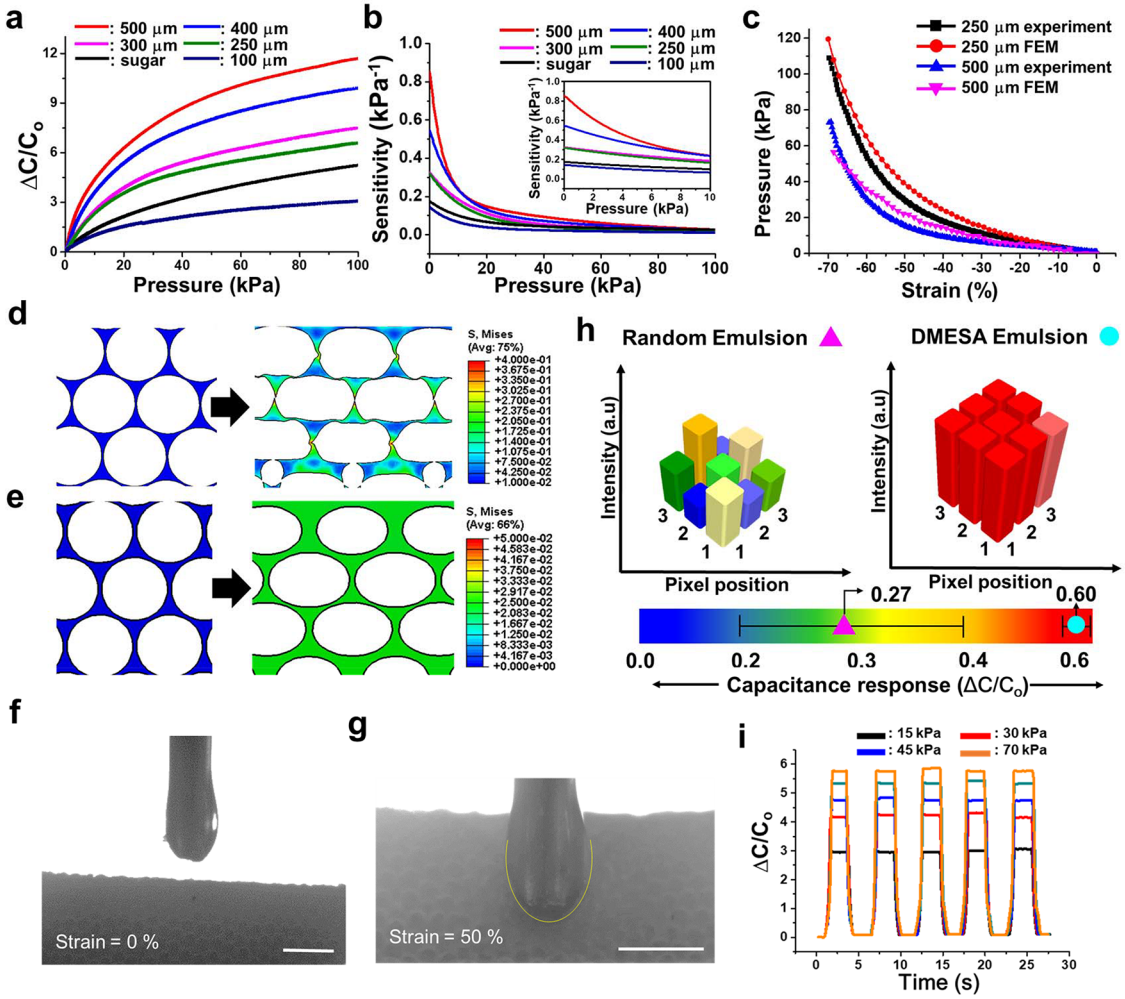

Figure 2. Characteristics of the capacitive pressure sensor fabricated using DMESA. (a) Relative capacitance change versus pressure curves for samples with different micropore sizes. (b) Sensitivity versus pressure curves for the samples with different micropore sizes. The inset shows a zoom-in of the pressure region <10 kPa. (c) Simulated and measured pressure versus strain curves of samples with micropore sizes of 250 and 500 μm. (D, E) Simulated (111) plane views of strained microstructures with (d) 500 μm and (e) 250 μm micropores under 30 kPa of pressure. (f, g) Photographs of the microstructured PDMS sample before (f) and after (g) being pressed by a tip with a diameter of 1 mm at 50% strain. The scale bar is 1 mm. (h) Relative capacitance change under 1.5 kPa pressure of a 3 × 3 array of 1 cm^2 samples fabricated using standard emulsion (left) and DMESA (right) process. (i) Relative capacitance change versus time plots for a sample with micropore size of 500 μm under various repeated pressures.

(Figure 1a, right). The gas permeability of PDMS[34] allows the 3D microporous structure to maintain its shape without collapsing when water evaporates, and this was confirmed by scanning electron microscopy (SEM) and optical microscopy images (Figure 1f,g). The pores had a coefficient of variation (CV) (ratio of standard deviation/average × 100%) of only 0.97%, verifying the high degree of pore size uniformity (Figure S1). As seen in Figure 1h,i, a 3 cm tall microstructured PDMS can easily be compressed by hand. Figure 1j shows large-area (9 cm in diameter) microstructured PDMS, fabricated in 30 min using four microfluidic channels simultaneously. The processing time can easily be shortened by implementing more microfluidic channels.

Characteristics of 3D Microstructured Elastomer-Based Capacitive Pressure Sensors. Capacitive pressure sensors were fabricated by using the microstructured elastomer itself as the active layer. We have prepared five samples with different pore sizes (100, 250, 300, 400, and 500 μm), and the relative capacitance change ($\Delta C/C_o$, where C_o is the initial capacitance and ΔC is the change in capacitance) versus pressure was measured for each sample (Figure 2a and Table S1). A sugar template-based porous PDMS sample was used as a reference (Figure S2).[24] The sensitivity versus pressure curves (Figure 2b) were obtained by taking the derivative of the curves in Figure 2a. For all of the samples, the sensitivity was relatively high at low pressures and gradually decreased as pressure increased. Interestingly, as the pore size increased from 100 to 500 μm, $\Delta C/C_o$ at 100 kPa increased by almost 4 factors, from 3.08 to 11.70 (Figure 2a). Also, as seen in Figure 2b, the sensitivity of the devices increased with increasing pore size, and the differences in the sensitivities were more pronounced in the low-pressure region and gradually decreased with increasing pressure. For the sample with 500 μm pore size, the sensitivity was as high as 0.86 kPa^{-1}, and the pressure as low as 10 Pa was detected (Figure S3).

To explain the aforementioned trends, a simulation tool (Abaqus FEA) was utilized to model the mechanical behavior of the samples with different pore sizes. Figure 2c shows the experimentally obtained and simulated pressure versus strain curves for samples with pore sizes 250 and 500 μm. The

DOI: 10.1021/acsami.8b19214
ACS Appl. Mater. Interfaces 2019, 11, 1503−1511

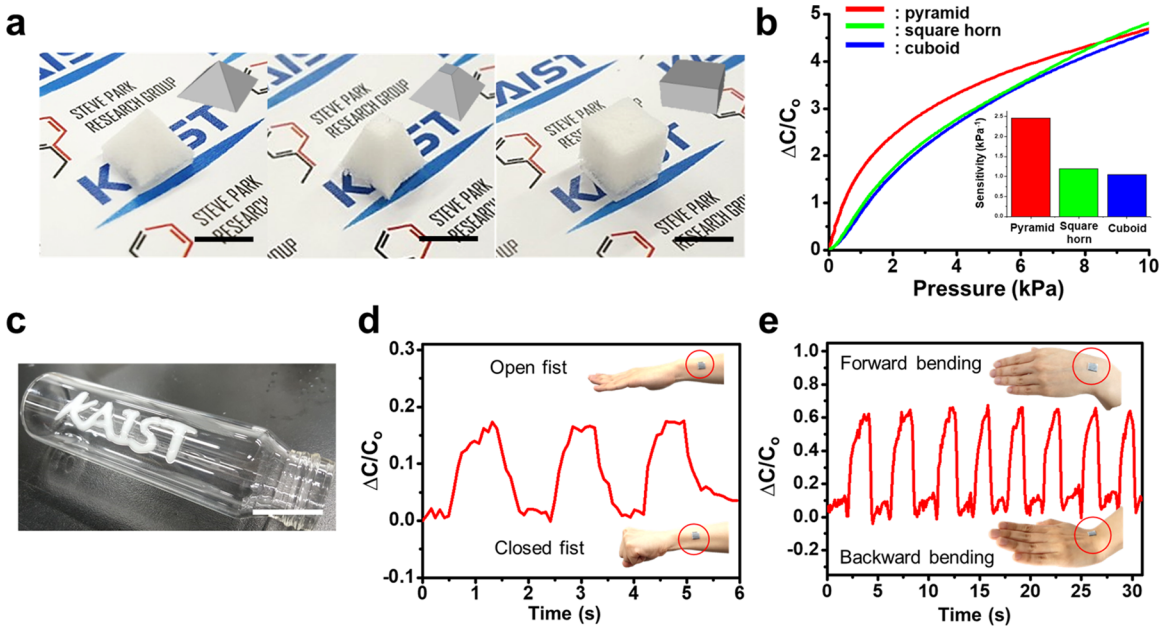

Figure 3. Versatile processability and human motion detection. (a) Photographs of different shapes of 3D microstructured elastomers: (left) pyramid, (middle) square horn, and (right) cuboid. The scale bar is 5 mm. (b) Relative capacitance change versus pressure curves for various shapes of microstructured pressure sensors. The inset shows the maximum sensitivity values for the different shapes of microstructured pressure sensors. (c) Nozzle-printed emulsion solution on a curved surface. The scale bar is 1 cm. (d, e) Relative capacitance change versus time plots demonstrating real-time monitoring of human motion: (d) closed and open fist and (e) forward and backward bending.

simulated pressure versus strain curves were similar to the experimentally measured curves. For both samples, the slope of the curves (i.e., compressive modulus) increases with increasing pressure, which explains why the sensitivity of the devices decreased with increasing pressure (i.e., sensitivity is inversely proportional to compressive modulus). The compressive modulus is low initially due to the presence of pores. However, as pressure is increased, the pores eventually collapse, after which the compressive modulus increases. Furthermore, the effective dielectric constant increases in the presence of pores at low pressures, since the volume fraction of air to PDMS constantly changes. Such an additional effect further increases the sensitivity of our sensor at low pressures.

Furthermore, the compressive modulus is smaller for the sample with larger pores than that with smaller pores. We can attribute this difference to the following. When a porous structure is compressed, the thin columns between two pores undergo an outward deflection called buckling. According to Euler's critical load, the critical force at which buckling occurs is inversely proportional to the length of the thin column between the pores.[35] Since the column of the larger pores is longer, buckling would occur at a relatively lower pressure; therefore, the sample with larger pores undergoes a larger strain than the sample with smaller pores at the same pressure. As seen in the simulated visual models (Figure 2d,e), under the same pressure, the sample with 500 μm pores shows collapsed pores due to buckling, whereas the sample with 250 μm pores remains uncollapsed. Under high pressures, the pores in both samples will be closed. Hence, the sensitivity of samples with different pore sizes will begin to merge as the structural effect of the different pore sizes will be lost (Figure 2b).

High spatial resolution and uniformity are other important properties of electronic skin applications. For high spatial resolution, it is desirable for only the contacted area to be compressed, while the surrounding area remains unstrained (i.e., low mechanical crosstalk). As seen in Figure 2f,g, when pressure is applied to the microstructured PDMS with a 1 mm diameter tip, only the area in contact is compressed. In contrast, when pressure is applied to an unstructured PDMS with the same tip, the surrounding area near the contacted area was simultaneously depressed (Figure S4). Figures 2h and S5 show a 3 × 3 taxel array made with 1 cm^2 devices using our DMESA technique on the right-hand side and using a standard emulsion technique with random sized pores on the left-hand side.[27] Since our pores are uniform in size and are assembled in an orderly manner, the characteristics of our devices were uniform in comparison. The coefficients of variation (ratio of standard deviation/average × 100%) in the relative capacitance change for the devices fabricated via DMESA and standard emulsion techniques were 2.8 and 24.6%, respectively. Such a high spatial resolution and uniformity will be highly useful for fabricating a dense array of taxels, which is currently an ongoing research.

Figure 2i shows $\Delta C/C_o$ versus time plots for a sensor with 500 μm pores under repeated loading and unloading of various pressures, which show the consistent capacitance change under each pressure. In addition, as seen in Figure S6, under a single cycle and even after 1000 cycles of loading and unloading at 70 kPa, our sensor exhibited consistent capacitance change, verifying the durability of our sensor. It is also notable that our sensor showed negligible hysteresis due to its micropores.[19] We hypothesized that the presence of micropores allows the structure to undergo deformation without causing long-range displacement of polymer chains, thereby reducing the viscoelastic behavior, which is the source of hysteresis. Our device had a response time shorter than 100 ms (Figure S7).

Versatile Processing and Human Motion Detection. Our 3D microstructure can itself be shaped using cast molding technique to further tune the sensing performance. Figures 3a and S8 show 3D microstructured elastomer shaped as a

DOI: 10.1021/acsami.8b19214
ACS Appl. Mater. Interfaces 2019, 11, 1503−1511

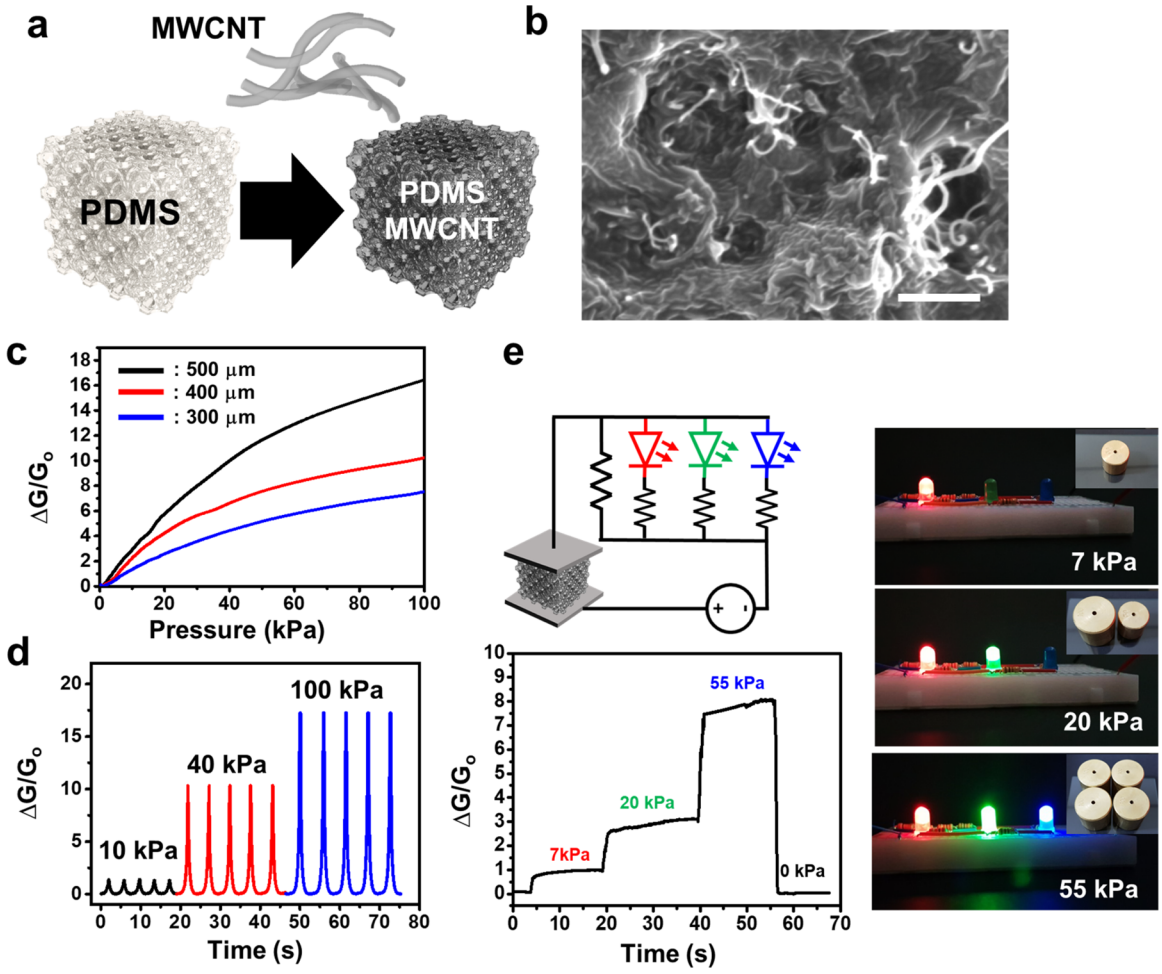

Figure 4. Three-dimensional microstructured MWCNT-based piezoresistive pressure sensor. (a) Schematic illustration of 3D microstructured PDMS functionalization with MWCNT. (b) SEM image of MWCNT-coated microstructured PDMS. The scale bar is 1 μm. (c) Relative conductance change versus pressure plots of MWCNT-coated microstructured PDMS samples with various micropore sizes. (d) Relative conductance change versus time plots for an MWCNT-coated microstructured PDMS with 500 μm micropores, under 10, 40, and 100 kPa of pressure. (e) Diagram and optical images of pressure-sensitive light-emitting diode (LED) circuit and relative conductance change versus time under various pressures. Different pressure levels yield different number of LEDs being turned on.

pyramid, square horn, and cuboid. Figure 3b shows the $\Delta C/C_o$ versus pressure curves and maximum sensitivities for the differently shaped samples, demonstrating that pyramid has the highest maximum sensitivity of 2.45 kPa^{-1}. Such high sensitivity is the combined effect of stress being concentrated at the vertex[20] and the relatively low compressive modulus of the microstructured PDMS. We have compared the compressive force versus strain curves and the stress distribution of the aforementioned shapes using Abaqus FEA simulation, and we have confirmed that pyramid has the lowest compressive modulus with the highest local stress (Figure S9). In addition, we demonstrate that our microstructured elastomer (in its liquid form, before PDMS curing and solvent evaporation) can be printed on a curved surface using nozzle printing (Figure 3c). These are highly advantageous features for future electronic skin applications such as wearable electronics and robotics.[36]

We have tested the human motion sensing capability of our device by attaching it onto the wrist of a human body, as shown in Figure S10 (Figure 3d,e). We first tested the difference in the signal with an open and closed fist. As seen in Figure 3d, when fist is repeatedly closed and opened, $\Delta C/C_o$ decreases and increases, respectively. The muscle contraction and expansion causes the device to expand laterally, which causes a change in the thickness of the microporous PDMS layer, hence resulting in the change in capacitance. We have also detected the bending motion of the wrist as seen in Figure 3e. The forward bending causes lateral expansion of the device and therefore a decrease in the thickness of the microporous PDMS, resulting in increase in capacitance. These demonstrations confirm that our device is sufficiently sensitive to detect subtle to large human motion.

Characteristics of Piezoresistive Pressure Sensors Based on MWCNT Functionalization. To fabricate piezoresistive pressure sensors, the 3D microstructured elastomers were functionalized with MWCNTs, as schematically depicted in Figure 4a. A 3D microstructured elastomer was immersed in MWCNT solution (solvent: toluene) for 10 min, taken out of the solution, and heated at 120 °C for 30 min to dry away the solvent. Attributed to the open network of the 3D microstructured elastomer and due to the swelling of PDMS in toluene (Figure S11), the MWCNT solution fully penetrated into the sample. This ultimately resulted in uniformly coated MWCNTs even in the innermost areas of the sample, as seen in the cross-sectional SEM image taken in the middle of the sample (Figure 4b). The MWCNTs were

DOI: 10.1021/acsami.8b19214
ACS Appl. Mater. Interfaces 2019, 11, 1503−1511

well adhered to the surface of PDMS, which stayed intact even under physical contact, such as rubbing with fingers or paper towel. Figure 4c and Table S2 show a plot and numerical analysis of relative conductance change ($\Delta G/G_o$) versus pressure for sensors made with different micropore sizes (i.e., since the applied voltage was 1 V, this is analogous to measuring current). As pressure is applied to the sensor, the conductance increases, which can be attributed to the increase in MWCNT connections as the pores are deformed.[37] The sensor with the largest micropore size of 500 μm showed the highest sensitivity of 0.34 kPa^{-1} in the pressure region <20 kPa and was able to detect pressure as low as 10 Pa (Figure S12). Again, the dependence of sensitivity on the micropore size can be ascribed to the difference in the compressive modulus of the microstructured elastomer, as explained above. Similar to the relative capacitance change measurements, the relative conductance change did not saturate up to 100 kPa. Figure 4d depicts a plot of $\Delta G/G_o$ versus time under the application and release of various pressures, demonstrating measurement reliability. We have also conducted 1000 cycles of loading and unloading at 70 kPa for the piezoresistive sensor, as depicted in Figure S13. Our piezoresistive sensor had a response time of about 5 ms (Figure S14).

One advantage of piezoresistive pressure sensors is their feasibility to be integrated with other components using simple electric circuits.[3] As a demonstration, we designed a pressure-controllable LED circuit, where applying different levels of pressure to the sensor controlled the number and color of LEDs being turned on and off (Figure 4e). Hence, the pressure being applied can easily be optically visualized.

Differentiation between Pressure, Temperature, and Proximity. One of the critical features needed in electronic skin is to differentiate between various external inputs. Here, we demonstrate that by simultaneously utilizing piezoresistive and capacitive pressure sensors (Figure S15), signals coming from pressure and temperature or from pressure and proximity can be distinguished. The networks of MWCNTs are known to be sensitive to temperature,[38] rendering our piezoresistive sensor responsive to both pressure and temperature (i.e., however, since both inputs result in resistance change, distinguishing between the two inputs is challenging). Capacitance is a measure of stored charge; hence, it is insensitive to temperature.[39] Therefore, by comparing the signals coming from the two sensors, temperature and pressure can be differentiated. The left-hand-side y-axis of Figure 5a shows a plot of relative resistance change of our piezoresistive sensor (i.e., ΔR is the change in resistance due to change in temperature and R_o is the resistance at 20 °C) under various pressure levels. These curves were well aligned with each other, meaning that temperature change can be measured at various pressure levels. The numerical analysis is shown in Table S3. Figure 5b shows a plot of relative resistance change and temperature as a function of time, showing decrease in resistance with increasing temperature. Such a trend has been reported previously in carbon nanotube-based bolometers.[40] Figure S16 in the Supporting Information depicts the response time of our piezoresistive sensor to temperature change. The right-hand-side y-axis of Figure 5a shows the capacitance of our capacitive pressure sensor as a function of temperature at various pressure levels, demonstrating its insensitivity to temperature at different pressure levels. Hence, the two types of sensors can be compared to simultaneously detect and distinguish between temperature and pressure.

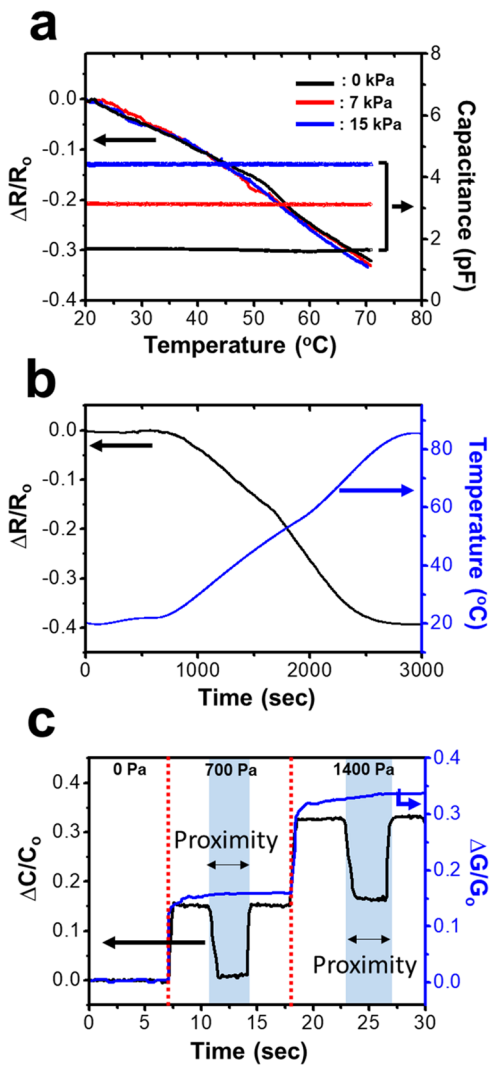

Figure 5. Differentiation of various inputs. (a) Relative resistance change due to temperature of our piezoresistive pressure sensor and capacitance of our capacitive pressure sensor as a function of temperature under various pressures. (b) Relative resistance change and temperature as a function of time. (c) Relative capacitance change of our capacitive pressure sensor and the relative conductance change of our piezoresistive pressure sensor as a function of time, simultaneously under pressure and proximity. The blue regions indicate proximity of finger near the sensors.

Another interesting feature of simultaneously using capacitive and piezoresistive pressure sensors is the ability to distinguish between proximity and pressure. Detecting proximity is a feature unique to capacitive sensors, which can be utilized to mimic hair follicle's sensory properties of human skin. When a conductive or dielectric material (e.g., human finger) comes near a capacitive sensor, the electric field lines are disturbed, resulting in a decrease in capacitance.[41] However, when the decrease in capacitance due to proximity is compensated by the increase in capacitance due to applied pressure, the resulting net relative capacitance change inaccurately depicts the current state of the sensor. As depicted on the left-hand-side y-axis of Figure 5c, approaching a human finger near the capacitive sensor (the blue regions) decreases the relative capacitance change by 0.15, which eliminates the increase in relative capacitance due to 700 Pa of pressure. To compensate for this inaccuracy, the piezoresistive sensor can be

DOI: 10.1021/acsami.8b19214
ACS Appl. Mater. Interfaces 2019, 11, 1503−1511

measured simultaneously, as depicted on the right-hand-side y-axis of Figure 5c. Evidently, the piezoresistive sensor is not responsive to proximity; hence, by comparing the signal coming from the two sensors, proximity and pressure can be accurately measured and distinguished. In addition, we have seen how strain affects the response of our sensors to pressure and temperature (Figure S17).

CONCLUSIONS

In this work, we have demonstrated the generation of 3D microstructured elastomer using droplet-based microfluidic-assisted emulsion self-assembly (DMESA) for the fabrication of high-performance pressure sensor for electronic skin applications. Our process can generate uniformly sized micropores assembled in an orderly close-packed manner over a large area. The size of the micropores can be easily controlled by tuning the relative flow rates of the oil- and water-based solutions. These features resulted in capacitive sensors with relatively high sensitivity (0.86 kPa^{-1}) and spatial uniformity. The increase in sensitivity with increasing pore size is attributed to relatively low pressure needed to induce buckling of larger microporous structure. We also showed that our 3D microstructure can be molded into different shapes and printed on curved surfaces. Furthermore, we have functionalized the microstructured elastomer with MWCNT to generate piezoresistive pressure sensors, which also exhibited relatively high sensitivity and large dynamic range. Finally, utilizing the two types of pressure sensors, we have differentiated between temperature and pressure and between pressure and proximity. We expect that our novel fabrication technique and unique device functionalities will be highly useful for enabling a wide variety of exciting electronic skin applications such as wearable electronics and robotics in the near future.

MATERIALS AND METHODS

Materials. Poly(dimethylsiloxane) (PDMS) was purchased from K1 solution. All chemical reactants were purchased from Sigma-Aldrich and used without any further purification. The PDMS oil solution was composed of the weight ratio of 1:1 PDMS and hexadecane containing 3 wt % span 80, and the solution was sonicated and degassed for 30 min prior to use. The aqueous solution was deionized water.

Fabrication of Microstructured PDMS. Microfluidic droplet generator devices were assembled using commercially available T-shape reactor and perfluoroalkoxyalkane tube (outer diameter, 1.0 m, and inner diameter, 500 μm). The volumetric flow rates of water and oil solutions were controlled by the speed of the syringe pumps (Harvard Apparatus). The formation of water emulsion droplets was analyzed using an optical microscope (MOTIC, BA310POL). The water emulsion droplets in PDMS oil solution were collected into a glass vial (dia. 1 cm) and heated to 80 °C for 3 h. This process evaporated the water and cured the PDMS. Thereafter, the sample was serially soaked in ethanol, isopropyl alcohol, and deionized water to completely remove oil residuals. The thickness of the sample was 5 mm. The surface and cross-sectional morphologies of the microstructured PDMS were characterized by optical microscopy and field emission scanning electron microscopy (Hitachi s4800).

Preparation of Microstructured PDMS for Capacitive Sensor. Indium tin oxide (ITO)-covered poly(ethylene terephthalate) (PET) substrates were used as flexible top and bottom electrodes. PDMS precursor containing 10 wt % curing agent was spin-coated (500 rpm for 5 s, followed by 1000 rpm for 30 s) on the ITO/PET substrates (on the ITO side) and was partially cured at 70 °C for 30 min. The thickness of this layer was 80 μm. Thereafter, microstructured PDMS was inserted between the ITO−PET substrates (the ITO side facing the microstructured PDMS) and was completely cured at 70 °C for 2 h. This firmly attached the ITO/PET substrates to the microstructured PDMS.

Spray Coating of Ag Nanowire on Microstructured PDMS Substrate. To fabricate the 3 × 3 array of electrodes, microstructured PDMS was placed on a hot plate preheated to 80 °C. Ag nanowire solution (1 wt %) was spray-coated with a metal stencil mask (10 mm opening with 5 mm spacing) placed on top of the microstructured PDMS. This process was repeated for the bottom side.

Nozzle Printing of Microstructured PDMS on a Curved Surface. To print on a curved surface, water droplets and oil solution were collected in a 20 mL syringe. The solution was then printed through a nozzle by applying pressure using a plunger.

Preparation of MWCNT Inks and Fabrication of the Piezoresistive Pressure Sensor. MWCNT solution was prepared by adding 15 mg of multiwalled carbon nanotube (Applied Carbon Nano Technology Co., Ltd.) and 15 mg of poly(3-dodecylthiophene-2,5-diyl) (P3DDT) (Rieke Metals) surfactant to 75 mL of toluene, followed by ultrasonication for 30 min at 70% amplitude. Microstructured PDMS was immersed in the MWCNT solution for 10 min, taken out of the solution, and heated at 120 °C for 30 min. The thickness of the sample was 5 mm. Indium tin oxide (ITO)-covered poly(ethylene terephthalate) (PET) substrates were used as flexible top and bottom electrodes using silver paste to attach the electrodes to the MWCNT-coated microstructured PDMS. The cross-sectional morphologies of the MWCNT-coated microstructured PDMS were characterized by field emission scanning electron microscopy (Hitachi s4800).

Fabrication of Various Shapes of Microstructured PDMS. Various shapes of microstructured PDMS (a pyramid, square horn, and cuboid) were fabricated via cast molding technique. The molds were made with polypropylene, fabricated using a 3D printer.

Numerical Simulation Detail. We utilized the ABAQUS explicit analysis to simulate the mechanical properties of porous PDMS sensors. For sensor geometry modeling, the pores were arranged as face-centered cubic crystal lattice to reflect the high porosity. The neo-Hookean constitutive model was used with a shear modulus of 30 kPa and a bulk modulus of 200 MPa. We used four-node linear tetrahedron elements with frictionless contact conditions in tangential and hard contact conditions in the normal direction. To satisfy the quasi-static simulation with minimal time cost, we used mass scaling to increase the simulation speed, while confirming that the kinetic energy of the model did not exceed 10% of the strain energy.

Characterization of Sensor Response. A high-precision universal test equipment (EMS 303) was employed to characterize the sensing performances of the microstructured PDMS sensors. The capacitance measurements were taken at a frequency of 1 MHz with a 1 V alternating current (AC) signal using an LCR meter (HP 4284A). The conductance and resistance measurements were taken at a frequency of 1 kHz with a 1 V AC signal using the same LCR meter. Force was controlled by a z-axis stage (10 μm resolution) loading bar with a force gauge (0.01 N resolution).

Statistical Analysis. For Figure 2h, the standard deviation was calculated using $s = \sqrt{\frac{\sum_{i=1}^{N}(x_i - \overline{x})^2}{N-1}}$, where s is the standard deviation, N is the number of sample measurements, and $\overline{x}$ is the mean value of the measurements. For the DMESA-based devices and the conventional emulsion-based devices, nine samples were measured for each type of device. The coefficient of variation (CV) was calculated using $CV = \frac{s}{\overline{x}} \times 100\%$, where s is the standard and $\overline{x}$ is the mean value of the measurements.

ASSOCIATED CONTENT

Supporting Information

The Supporting Information is available free of charge on the ACS Publications website at DOI: 10.1021/acsami.8b19214.

DOI: 10.1021/acsami.8b19214
ACS Appl. Mater. Interfaces 2019, 11, 1503−1511

Numerical analysis on the capacitive pressure-sensing performance, piezoresistive pressure-sensing performance, piezoresistive temperature-sensing performance (Tables S1−S3); pore size distribution from SEM image analysis; SEM image of sugar template-based microstructure; limit of detection of the capacitive pressure sensor; bare PDMS sample pressed by a 1 mm diameter tip, schematic and optical images of a 3 × 3 array device; cyclic stability of a 500 μm microporous capacitive sensor; response time of a 500 μm pore capacitive sensor; different shapes of 3D microstructured elastomers; simulation of various shapes of 3D microstructured PDMS; 3D porous PDMS film detecting human motion; optical image of swollen 3D microstructured PDMS in MWCNT solution; limit of detection of the capacitive pressure sensor; cyclic stability of a 500 μm microporous piezoresistive sensor; response time of a 500 μm pore piezoresistive sensor; optical image of an integrated sensor; response of a piezoresistive sensor under rapid change in temperature; response of the capacitive and piezoresistive sensors under strain (Figures S1−S17) (PDF)

■ AUTHOR INFORMATION

Corresponding Author

*E-mail: stevepark@kaist.ac.kr.

ORCID

Steve Park: 0000-0002-1428-592X

Author Contributions

[‖]J.-O.K. and S.Y.K. contributed equally to this work.

Notes

The authors declare no competing financial interest.

■ ACKNOWLEDGMENTS

J.-O.K. and S.Y.K. equally contributed to this work. This work was supported by the National Research Foundation of Korea (NRF) grant funded by the Korea government (MSIT) (No. 2016RlC1B1009949) and KAIST grant funded by the Ministry of Science and ICT.

■ REFERENCES

(1) Schwartz, G.; Tee, B. C.; Mei, J.; Appleton, A. L.; Kim, D. H.; Wang, H.; Bao, Z. Flexible Polymer Transistors with High Pressure Sensitivity for Application in Electronic Skin and Health Monitoring. *Nat. Commun.* **2013**, *4*, No. 1859.

(2) Ramuz, M.; Tee, B. C.; Tok, J. B.; Bao, Z. Transparent, Optical, Pressure-Sensitive Artificial Skin for Large-Area Stretchable Electronics. *Adv. Mater.* **2012**, *24*, 3223−3227.

(3) Zang, Y.; Zhang, F.; Di, C.-a.; Zhu, D. Advances of Flexible Pressure Sensors toward Artificial Intelligence and Health Care Applications. *Mater. Horiz.* **2015**, *2*, 140−156.

(4) Hammock, M. L.; Chortos, A.; Tee, B. C.-K.; Tok, J. B.-H.; Bao, Z. 25th Anniversary Article: The Evolution of Electronic Skin (E-Skin): A Brief History, Design Considerations, and Recent Progress. *Adv. Mater.* **2013**, *25*, 5997−6038.

(5) Miyamoto, A.; Lee, S.; Cooray, N. F.; Lee, S.; Mori, M.; Matsuhisa, N.; Jin, H.; Yoda, L.; Yokota, T.; Itoh, A.; Sekino, M.; Kawasaki, H.; Ebihara, T.; Amagai, M.; Someya, T. Inflammation-Free, Gas-Permeable, Lightweight, Stretchable On-Skin Electronics with Nanomeshes. *Nat. Nanotechnol.* **2017**, *12*, 907−913.

(6) Someya, T.; Sekitani, T.; Iba, S.; Kato, Y.; Kawaguchi, H.; Sakurai, T. A Large-Area, Flexible Pressure Sensor Matrix with Organic Field-Effect Transistors for Artificial Skin Applications. *Proc. Natl. Acad. Sci. U.S.A.* **2004**, *101*, 9966−9970.

(7) Kim, J.; Lee, M.; Shim, H. J.; Ghaffari, R.; Cho, H. R.; Son, D.; Jung, Y. H.; Soh, M.; Choi, C.; Jung, S.; Chu, K.; Jeon, D.; Lee, S.-T.; Kim, J. H.; Choi, S. H.; Hyeon, T.; Kim, D.-H. Stretchable Silicon Nanoribbon Electronics for Skin Prosthesis. *Nat. Commun.* **2014**, *5*, No. 5747.

(8) Rogers, J. A.; Someya, T.; Huang, Y. Materials and Mechanics for Stretchable Electronics. *Science* **2010**, *327*, 1603−1607.

(9) Zeng, W.; Shu, L.; Li, Q.; Chen, S.; Wang, F.; Tao, X. M. Fiber-Based Wearable Electronics: A Review of Materials, Fabrication, Devices, and Applications. *Adv. Mater.* **2014**, *26*, 5310−5336.

(10) Pantelopoulos, A.; Bourbakis, N. G. A Survey on Wearable Sensor-Based Systems for Health Monitoring and Prognosis. *IEEE Trans. Syst., Man, Cybern. C, Appl. Rev.* **2010**, *40*, 1−12.

(11) Sadasivuni, K. K.; Kafy, A.; Zhai, L.; Ko, H. U.; Mun, S.; Kim, J. Transparent and Flexible Cellulose Nanocrystal/Reduced Graphene Oxide Film for Proximity Sensing. *Small* **2015**, *11*, 994−1002.

(12) Wang, X.; Gu, Y.; Xiong, Z.; Cui, Z.; Zhang, T. Silk-Molded Flexible, Ultrasensitive, and Highly Stable Electronic Skin for Monitoring Human Physiological Signals. *Adv. Mater.* **2014**, *26*, 1336−1342.

(13) Trivedi, D.; Rahn, C. D.; Kier, W. M.; Walker, I. D. Soft Robotics: Biological Inspiration, State of the Art, and Future Research. *Appl. Bionics Biomech.* **2008**, *5*, 99−117.

(14) Webb, R. C.; Bonifas, A. P.; Behnaz, A.; Zhang, Y.; Yu, K. J.; Cheng, H.; Shi, M.; Bian, Z.; Liu, Z.; Kim, Y. S.; Yeo, W. H.; Park, J. S.; Song, J.; Li, Y.; Huang, Y.; Gorbach, A. M.; Rogers, J. A. Ultrathin Conformal Devices for Precise and Continuous Thermal Characterization of Human Skin. *Nat. Mater.* **2013**, *12*, 938−944.

(15) Tee, B. C.-K.; Wang, C.; Allen, R.; Bao, Z. An Electrically and Mechanically Self-Healing Composite with Pressure- and Flexion-Sensitive Properties for Electronic Skin Applications. *Nat. Nanotechnol.* **2012**, *7*, 825−832.

(16) Hua, Q.; Sun, J.; Liu, H.; Bao, R.; Yu, R.; Zhai, J.; Pan, C.; Wang, Z. L. Skin-Inspired Highly Stretchable and Conformable Matrix Networks for Multifunctional Sensing. *Nat. Commun.* **2018**, *9*, No. 244.

(17) Sarwar, M. S.; Dobashi, Y.; Preston, C.; Wyss, J. K. M.; Mirabbasi, S.; Madden, J. D. W. Bend, Stretch, and Touch: Locating a Finger on an Actively Deformed Transparent Sensor Array. *Sci. Adv.* **2017**, *3*, No. e1602200.

(18) Yamamoto, Y.; Harada, S.; Yamamoto, D.; Honda, W.; Arie, T.; Akita, S.; Takei, K. Printed Multifunctional Flexible Device with an Integrated Motion Sensor for Health Care Monitoring. *Sci. Adv.* **2016**, *2*, No. e1601473.

(19) Mannsfeld, S. C. B.; Tee, B. C. K.; Stoltenberg, R. M.; Chen, C. V. H. H.; Barman, S.; Muir, B. V. O.; Sokolov, A. N.; Reese, C.; Bao, Z. Highly Sensitive Flexible Pressure Sensors with Microstructured Rubber Dielectric Layers. *Nat. Mater.* **2010**, *9*, 859−864.

(20) Tee, B. C.-K.; Chortos, A.; Dunn, R. R.; Schwartz, G.; Eason, E.; Bao, Z. Tunable Flexible Pressure Sensors using Microstructured Elastomer Geometries for Intuitive Electronics. *Adv. Funct. Mater.* **2014**, *24*, 5427−5434.

(21) Pan, L.; Chortos, A.; Yu, G.; Wang, Y.; Isaacson, S.; Allen, R.; Shi, Y.; Dauskardt, R.; Bao, Z. An Ultra-Sensitive Piezoresistive Pressure Sensor Based on Hollow-Sphere Microstructure Induced Elasticity in Conducting Polymer Film. *Nat. Commun.* **2014**, *5*, No. 3002.

(22) Choong, C. L.; Shim, M. B.; Lee, B. S.; Jeon, S.; Ko, D. S.; Kang, T. H.; Bae, J.; Lee, S. H.; Byun, K. E.; Im, J.; Jeong, Y. J.; Park, C. E.; Park, J. J.; Chung, U. I. Highly Stretchable Piezoresistive Pressure Sensors Using a Conductive Elastomeric Composite on a Micropyramid Array. *Adv. Mater.* **2014**, *26*, 3451−3458.

(23) Kwon, D.; Lee, T. I.; Shim, J.; Ryu, S.; Kim, M. S.; Kim, S.; Kim, T. S.; Park, I. Highly Sensitive, Flexible, and Wearable Pressure Sensor Based on a Giant Piezocapacitive Effect of Three-Dimensional Microporous Elastomeric Dielectric Layer. *ACS Appl. Mater. Interfaces* **2016**, *8*, 16922−16931.

(24) Rinaldi, A.; Tamburrano, A.; Fortunato, M.; Sarto, M. S. A Flexible and Highly Sensitive Pressure Sensor Based on a PDMS

DOI: 10.1021/acsami.8b19214
ACS Appl. Mater. Interfaces 2019, 11, 1503−1511

Foam Coated with Graphene Nanoplatelets. *Sensors* **2016**, *16*, No. 2148.
(25) Choi, S.-J.; Kown, T.-H.; Im, H.; Moon, D.-I.; Baek, D. J.; Seol, M.-L.; Duarte, J. P.; Choi, Y.-K. A Polydimethylsiloxane (PDMS) Sponge for the Selective Absorption of Oil from Water. *ACS Appl. Mater. Interfaces* **2011**, *3*, 4552−4556.
(26) Kang, S.; Lee, J.; Lee, S.; Kim, S.; Kim, J.-K.; Algadi, H.; Al-Sayari, S.; Kim, D.-E.; Kim, D.; Lee, T. Highly Sensitive Pressure Sensor Based on Bioinspired Porous Structure for Real-Time Tactile Sensing. *Adv. Electron. Mater.* **2016**, *2*, No. 1600356.
(27) Yang, C.; Xu, Y.; Man, P.; Zhang, H.; Huo, Y.; Yang, C.; Li, Z.; Jiang, S.; Man, B. Formation of Large-Area Sretchable 3D Graphene−Nickel Particle Foams and Their Sensor Applications. *RSC Adv.* **2017**, *7*, 35016−35026.
(28) Chen, M.; Zhang, L.; Duan, S.; Jing, S.; Jiang, H.; Li, C. Highly Stretchable Conductors Integrated with a Conductive Carbon Nanotube/Graphene Network and 3D Porous Poly(dimethylsiloxane). *Adv. Funct. Mater.* **2014**, *24*, 7548−7556.
(29) Kim, K. N.; Lee, J. P.; Lee, S. H.; Lee, S. C.; Baik, J. M. Ergonomically Designed Replaceable and Multifunctional Triboelectric Nanogenerator for a Uniform Contact. *RSC Adv.* **2016**, *6*, 88526−88530.
(30) Yang, L.; Wang, R.; Song, Q.; Liu, Y.; Zhao, Q.; Shen, Y. One-Pot Preparation of Porous Piezoresistive Sensor with High Strain Sensitivity via Emulsion-Templated Polymerization. *Composites, Part A* **2017**, *101*, 195−198.
(31) Kovalenko, A.; Zimny, K.; Mascaro, B.; Brunet, T.; Mondain-Monval, O. Tailoring of the Porous Structure of Soft Emulsion-Templated Polymer Materials. *Soft Matter* **2016**, *12*, 5154−5163.
(32) Jung, S.; Kim, J. H.; Kim, J.; Chio, S.; Lee, J.; Park, I.; Hyeon, T.; Kim, D.-H. Reverse-Micelle-Induced Porous Pressure-Sensitive Rubber for Wearable Human-Machine Interfaces. *Adv. Mater.* **2014**, *26*, 4825−4830.
(33) Tadros, T. F. *Emulsion Formation and Stability*; Tadros, T. F., Ed.; Wiley: Weinheim, Germany, 2013; Chapter 1, pp 1−75.
(34) Firpo, G.; Angeli, E.; Repetto, L.; Valbusa, U. Permeability Thickness Dependence of Polydimethylsiloxane (PDMS) Membranes. *J. Membr. Sci.* **2015**, *481*, 1−8.
(35) Cote, F.; Biagi, R.; Bart-Smith, H.; Deshpande, V. S. Structural Response of Pyramidal Core Sandwich Columns. *Int. J. Solids Struct.* **2007**, *44*, 3533−3556.
(36) Ha, M.; Lim, S.; Ko, H. Wearable and Flexible Sensors for User-Interactive Health-Monitoring Devices. *J. Mater. Chem. B* **2018**, *6*, 4043−4064.
(37) Huang, W.; Dai, K.; Zhai, Y.; Liu, H.; Zhan, P.; Gao, J.; Zheng, G.; Liu, C.; Shen, C. Flexible and Lightweight Pressure Sensor Based on Carbon Nanotube/Thermoplastic Polyurethane-Aligned Conductive Foam with Superior Compressibility and Stability. *ACS Appl. Mater. Interfaces* **2017**, *9*, 42266−42277.
(38) Neitzert, H. C.; Vertuccio, L.; Sorrentino, A. Epoxy/MWCNT Composite as Temperature Sensor and Electrical Heating Element. *IEEE Trans. Nanotechnol.* **2011**, *10*, 688−693.
(39) Dempsey, S. J.; Szablewski, M.; Atkinson, D. Tactile Sensing in Human−Computer Interfaces: The Inclusion of Pressure Sensitivity as a Third Dimension of User Input. *Sens. Actuators, A* **2015**, *232*, 229−250.
(40) Lu, R.; Shi, J. J.; Baca, F. J.; Wu, J. Z. High Performance Multiwall Carbon Nanotube Bolometers. *J. Appl. Phys.* **2010**, *108*, No. 084305.
(41) Kulkarni, M. R.; John, R. A.; Rajput, M.; Tiwari, N.; Yantara, N.; Nguyen, A. C.; Mathews, N. Transparent Flexible Multifunctional Nanostructured Architectures for Non-optical Readout, Proximity, and Pressure Sensing. *ACS Appl. Mater. Interfaces* **2017**, *9*, 15015−15021.

DOI: 10.1021/acsami.8b19214
ACS Appl. Mater. Interfaces 2019, 11, 1503−1511